# Mechanisms generating bistability and oscillations in microRNA-mediated motifs

Peipei Zhou,[1,*] Shuiming Cai,[1,2,*] Zengrong Liu,[1,2] and Ruiqi Wang[1,†]
[1]*Institute of Systems Biology, Shanghai University, Shanghai 200444, China*
[2]*Department of Mathematics, Shanghai University, Shanghai 200444, China*
(Received 22 December 2011; published 23 April 2012)

The importance of post-transcriptional regulation by microRNAs (miRNAs) has recently been recognized in almost all cellular processes. When participating in cellular processes, miRNAs mainly mediate mRNA degradation or translational repression. Recently computational and experimental studies have identified an abundance of motifs involving miRNAs and transcriptional factors (TFs). The simplest motif is a two-node miRNA-mediated feedback loop (MFL) in which a TF regulates an miRNA and the TF itself is negatively regulated by the miRNA. In this paper we present a general computational model for the MFL based on biochemical regulations and explore its dynamics by using bifurcation analysis. Our results show that the MFL can behave either as switches or as oscillators, depending on the TF as a repressor or an activator. These functional features are consistent with the widespread appearance of miRNAs in fate decisions such as proliferation, differentiation, and apoptosis during development. We found that under the interplay of a TF and an miRNA, the MFL model can behave as switches for wide ranges of parameters even without cooperative binding of the TF. In addition, oscillations induced by the miRNA in the MFL model require neither an additional positive feedback loop, nor self-activation of the gene, nor cooperative binding of the TF, nor saturated degradation. Therefore, the MFL may provide a general network structure to induce bistability or oscillations. It is hoped that the results presented here will provide a new view on how gene expression is regulated by miRNAs and further guidance for experiments. Moreover, the insight gained from this study is also expected to provide a basis for the investigation of more complex networks assembled by simple building blocks.

DOI: 10.1103/PhysRevE.85.041916 PACS number(s): 87.17.Aa, 87.16.Yc, 82.40.Bj

## I. INTRODUCTION

In the past, it was believed that the regulation of gene expression is a task of regulatory proteins in all organisms, and thus most research on gene regulation focused mainly on transcriptional and post-translational regulations. In recent years, a post-transcriptional regulation manifested by small noncoding RNAs is being uncovered due to the development of large-scale experimental and computational techniques. It has been recognized that the post-transcriptional regulation plays important roles in the regulation of many cellular processes [1,2].

MicroRNAs (miRNAs) are a class of ∼22-nucleotide noncoding RNAs that are expected to target a substantial portion of eukaryote genome [3] and have been shown to play crucial roles in almost all biological processes ranging from development and metabolism to apoptosis and signaling pathways [4–6]. An miRNA regulates gene expression post-transcriptionally through canonical base pairing to its target mRNAs at conserved sites in the 3′ untranslated regions, ultimately leading to a reduction in the levels of proteins encoded by the target mRNAs [7]. Substantial evidence suggests that the suppression can occur by either translational repression or mRNA cleavage [7–10]. Although it has been shown that miRNAs can potentially bind and silence hundreds of mRNAs across a number of signaling pathways to integrate multiple genes into biologically meaningful networks and regulate a variety of cellular processes, the mechanisms of various functions and biological significance of miRNAs are still not well understood [11–33].

Large-scale statistical analysis of transcriptional regulatory networks in the bacterium *Escherichia coli* [34] and the budding yeast *Saccharomyces cerevisiae* [35] has uncovered significantly recurring nontrivial patterns of interconnections termed network motifs contained in these networks. Each motif has been suggested to have a specified structure and capacity to perform specific information-processing functions [36–38]. Familiar examples of motifs include (1) negative autoregulation, which enables homeostasis and increases response time in gene circuits [39], and linearizes the dose response and suppresses the heterogeneity of gene expression [37]; (2) coherent feed-forward loops, which can introduce a time delay in activation as well as detect persistence in input signals [40]; and (3) incoherent feed-forward loops, which can function as pulse generators [41], response accelerators [42], and fold-change detectors in gene regulation [38]. These motifs may also act in combination to generate more complex regulatory patterns in transcriptional networks [36]. Moreover, it has been found that, in many systems studied so far, the motifs are linked to each other in a way that does not spoil the independent function of each motif [36], which suggests that network dynamics might be understood as combinations of these elementary computational units [43].

Recently several studies have shown that the transcriptional regulation by transcription factors (TFs) and post-transcriptional regulation by miRNAs are often highly coordinated [11–19]. These results imply that the existence of considerable crosstalk between the transcriptional and post-transcriptional layers. Therefore, miRNA functions can be fully understood only by integrating TF and miRNA regulations into "mixed" networks. As in the case of purely

*Peipei Zhou and Shuiming Cai contributed equally to this work.
†rqwang@shu.edu.cn

 


FIG. 1. (Color online) Schematic illustration of the overrepresented MFL motif [11–13,16–19]. The solid and dotted lines represent transcriptional and posttranscriptional regulations, respectively.

transcriptional networks [36,44], several recurrent network motifs have also been detected in these mixed networks [11–19]. The simplest motif is a two-node miRNA-mediated feedback loop (MFL) comprising both transcriptional and post-transcriptional regulation, as shown in Fig. 1 and further in Fig. 3. In this motif, the protein $A$ produced from gene $g_a$ regulates the transcription of miRNA gene $g_s$, and the miRNA transcribed from gene $g_s$ negatively regulates gene $g_a$ post-transcriptionally. The MFL can be classified into two classes: coherent (double negative) and incoherent (single negative) feedback loops [17,36], depending on the kind of the transcriptional regulations.

In this paper, we focus on two particular network motifs: the miRNA-mediated double negative feedback loop (MDNFL) in which a TF suppresses an miRNA and the TF itself is negatively regulated by the miRNA, and the miRNA-mediated single negative feedback loop (MSNFL) in which a TF activates an miRNA and the TF itself is negatively regulated by the miRNA. The major motivation of this study is that these specific motifs have been reported in some recent studies [22–31] (Fig. 2). For example, in human hematopoietic cells, NFI-A and miR-233 function in a double negative feedback loop to control granulocytic differentiation [22] [Fig. 2(a)]. In *Drosophila* eye development, the reciprocal repression between Yan and miR-7 ensures their mutually exclusive expression pattern [23] [Fig. 2(b)]. In addition, a double negative feedback loop between the antineural REST/SCP1 and proneural miR-124 pathways contributes to a rapid and efficient transition of cellular phenotypes between neural progenitors and postmitotic neurons during embryonic central nervous system development [24] [Fig. 2(c)]. Likewise, ZEB1/SIP1 and the miR-200 family form a double negative feedback loop to regulate epithelial-mesenchymal transition during embryological development [25] [Fig. 2(d)]. Upon initiation of embryonic stem cell differentiation, reciprocal inhibition of miR-145 and OCT4 contributes to irreversible silencing of self-renewal and pluripotency programs [26] [Fig. 2(e)]. Ezh2 and miR-214 function in a double negative feedback loop to regulate skeletal muscle cell differentiation during skeletal muscle development [27] [Fig. 2(f)]. TLX and miR-9 form a double negative feedback loop to control the balance between neural stem cell proliferation and differentiation [28] [Fig. 2(g)]. Moreover, mutual inhibition of Egr2 and miR-17-92 regulates PU.1-directed macrophage differentiation [29] [Fig. 2(h)]. In the E2F1/miR-17-20/c-Myc network in human, the module E2F1/miR-17-20 belongs to the MSNFL motif, in which E2F1 activates transcription of the miR-17-20 miRNA cluster and miR-17-20 mediates a negative feedback to E2F1 [11] [Fig. 2(i)]. Another MSNFL motif is the module LIN-26/miR-43 in *C. elegans*, in which LIN-26 activates expression of miR-34 and miR-34 in turn post-transcriptionally suppresses synthesis of LIN-26 [16] [Fig. 2(j)]. Similar MSNFL motifs are also found in human hematopoietic [30] [Fig. 2(k)] and breast cancer cells [31] [Fig. 2(l)].

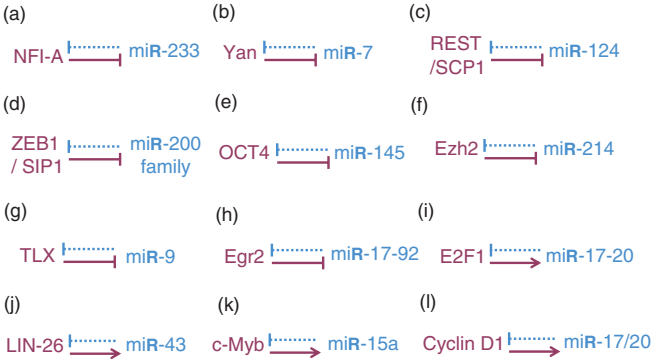


FIG. 2. (Color online) Biological examples of the MFL motif. (a) MDNFL controls granulocytic differentiation in human hematopoietic cells [22]. (b) MDNFL promotes photoreceptor differentiation in the *Drosophila* eye [23]. (c) MDNFL contributes to a rapid and efficient transition of cellular phenotypes between neural progenitors and postmitotic neurons during embryonic central nervous system development [24]. (d) MDNFL regulates epithelial-mesenchymal transition during embryological development [25]. (e) MDNFL contributes to irreversible silencing of self-renewal and pluripotency programs upon initiation of embryonic stem cell differentiation [26]. (f) MDNFL regulates skeletal muscle cell differentiation during skeletal muscle development [27]. (g) MDNFL controls the balance between neural stem cell proliferation and differentiation [28]. (h) MDNFL regulates PU.1-directed macrophage differentiation [29]. (i) MSNFL regulates the balance between cell proliferation and apoptosis [11]. (j) MSNFL in *C. elegans* [16]. (k) MSNFL in human hematopoietic cells [30]. (l) MSNFL in the control of breast cancer cell proliferation [31].

It has been shown that double negative feedback loop can serve as bistable switches both experimentally and theoretically [45–48]. In this way, it can convert a transient signal into a longer-lasting cellular response: once one of two alternative states is established, the signaling cue which induces the transition is no longer necessary and the status is maintained by itself. In addition, it has also been shown that single negative feedback loop can induce oscillations [49]. However, it is not clear whether the MDNFL (MSNFL) can similarly behave as a bistable switch (an oscillator) and further the possible functions and biological significance of the miRNA in the MDNFL (MSNFL).

To address these questions, we construct a general computational model of the MFL based on biochemical regulations. Detailed analysis of the model reveals that there exist wide ranges of kinetic parameters where the MDNFL (MSNFL) can behave as bistable switches (oscillators). These functional features are consistent with the widespread appearance of miRNAs in fate decisions such as proliferation, differentiation, and apoptosis during development. It is hoped that the results presented here will provide a new view of how gene expression is regulated by miRNAs and further guidance for experiments. Moreover, the insight gained from this study is also expected to provide a basis for the investigation of more complex networks assembled by simple modules.

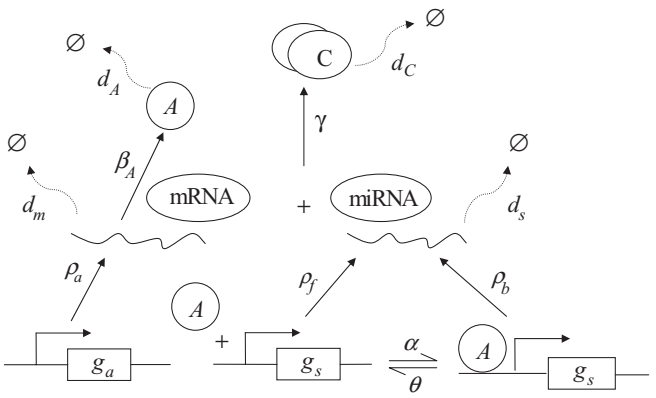


FIG. 3. The proposed model of the MFL motif. The Greek letters denote different parameters of the model.

## II. A MATHEMATICAL MODEL OF THE MFL

The MFL consists of two genes $g_a$, $g_s$, their corresponding transcripts, mRNA, miRNA, and a protein $A$ encoded by $g_a$, as shown in Fig. 3. The protein $A$ regulates transcription of gene $g_s$ and the miRNA base pairs with the mRNA. It is worth mentioning that the mechanisms of microRNA-mediated gene regulation can be translational repression or destablization of its target mRNAs [9]; i.e., the miRNA can either decrease the rate of translation or increase the degradation of its target mRNAs. Here we choose to model the effect of miRNA regulation by taking the degradation rate of the mRNA as a function of miRNA concentration. The alternative choice of modeling the effect of miRNA regulation by taking the degradation rate of the protein $A$ as a function of miRNA concentration yields similar results, as reported in the Appendix.

The time evolution of the concentrations of these species can be described by the rate equations as follows:

$$\frac{d[g_s]}{dt} = \theta[g_s{:}A] - \alpha[g_s][A], \tag{1}$$

$$\frac{d[M_s]}{dt} = \rho_f[g_s] + \rho_b[g_s:A] - d_s[M_s] - \gamma[M_a][M_s], \tag{2}$$

$$\frac{d[M_a]}{dt} = \rho_a - d_m[M_a] - \gamma[M_a][M_s], \tag{3}$$

$$\frac{d[A]}{dt} = \beta_A[M_a] - d_A[A] + \theta[g_s:A] - \alpha[A][g_s], \tag{4}$$

where $[g_s]$, $[g_s:A]$, $[M_s]$, $[M_a]$, and $[A]$ denote the concentration of free gene $g_s$, gene $g_s$ with $A$ bound to its promoter, miRNA, mRNA, and protein $A$, respectively. Here the cell volume is taken as the volume unit, and thus the concentration of a species can also represent its effective number present in the cell, as adopted in Ref. [50]. It is assumed that the total binding sites of the promoter to be constant, i.e., $[g_s] + [g_s:A] = 1$ mol. Therefore, $[g_s]$ can also represent the probability that gene $g_s$ is free without $A$ bound to its promoter. Specifically, protein $A$ binds to the promoter of gene $g_s$ at a rate $\alpha$, and when bound they dissociate at a rate $\theta$. The miRNA $M_s$ is produced at a rate $\rho_b$ when $A$ binds to gene $g_s$ or at a rate $\rho_f$ otherwise. Thus, $\rho_b < \rho_f$ corresponds to transcriptional repression by $A$ and $\rho_b > \rho_f$ to transcriptional activation. For the first case, the motif is a MDNFL one, and for the latter case, a MSNFL motif. Since regulation of gene $g_a$ is not considered, it is simply assumed that mRNA $M_a$ is produced at a given basal rate $\rho_a$. The mRNA $M_a$ produces protein $A$ at a rate $\beta_A$. $d_s$, $d_m$, and $d_A$ are the degradation rates of $M_s$, $M_a$, and $A$, respectively. The miRNA base pairs with the mRNA at a rate $\gamma$. The base pairing blocks the binding of the ribosome to the mRNA, thus mediating mRNA degradation [13]. According to the fact that the complex formed by miRNA and mRNA is extremely stable or rapidly degraded, we assume that the base pairing is irreversible and thus the complex needs not to be treated as a dynamical variable. It is worth mentioning that how many copies of a TF bind to the miRNA promoter is often unclear. There may be one, two, or even more TF binding sites. Here we consider just the case of one TF binding site, i.e., without cooperativity. When further information about the binding sites is known, cooperative binding and Hill functions can be taken into account, and similar analysis can be performed [51].

There are ten parameters in the model, and possible ranges of their values should be provided to guide model analysis. In general, the range of each parameter value is rather wide. Half-lives of mRNA range from a few minutes to several hours and are peaked around 20 min in yeast [52,53]. We therefore choose $d_m = 0.05$ min$^{-1}$ as a typical value. Protein half-lives vary from a few minutes to several days [53,54], and we therefore choose $d_A = 0.01$ min$^{-1}$ as a standard value. More generally, we assume that half-life of the protein is longer than that of its mRNA [50]. Based on the fact that miRNAs are generally more stable than proteins [55,56], we assume that $d_s = 0.005$ min$^{-1}$. For the TF-promoter interaction, typical values appear to be a critical concentration $\theta/\alpha = [A]_0$ in the nanomolar range, a bound state lifetime of several minutes, and activated transcription rates of a few mRNAs per minute [50]. Therefore, we assume that $\alpha = \theta/40$ and $\theta$ has the same order as $d_m$, and $\rho_f$ and $\rho_b$ range from 0.1 mol min$^{-1}$ to 100 mol min$^{-1}$ [13,50]. The basal transcription rate of mRNA $\rho_a$ ranges from 0.1 mol min$^{-1}$ to 10 mol min$^{-1}$ [50,57]. For the protein production, we assume that $\beta_A = 1$ min$^{-1}$, which means that one protein molecule is translated from one mRNA molecule per minute. The value of $\gamma$ has been estimated to be around 0.02 mol$^{-1}$min$^{-1}$ for several miRNA/target pairs [57,58]. Thus, $\gamma = 0.02$ mol$^{-1}$min$^{-1}$ is taken as a typical value.

## III. RESULTS

Intuitively, when the transcription rate of the miRNA is larger than that of the mRNA, irrespective of the state of the $g_s$ promoter, i.e., $\rho_a < \rho_f$ and $\rho_a < \rho_b$, more miRNA molecules are transcribed than mRNA and most of mRNA molecules are expected to base pair rapidly with the miRNA molecules and degraded, which will result in a low expression of protein $A$. In this case the system with any initial condition will converge to a single stable state. Similarly, an opposite result holds when both transcription rates of miRNA are smaller than that of mRNA, i.e., $\rho_b < \rho_a$ and $\rho_f < \rho_a$. In this case, the number of mRNA molecules greatly exceeds that of miRNA molecules, and only a small fraction of the total mRNA molecules are codegraded with miRNA. Thus, mRNA molecules are accumulated and translated into proteins, which leads to a high protein $A$ level. Interestingly, the system

dynamics will become complex when the transcription rate of mRNA is intermediate between the two transcription rates of the miRNA, i.e., $\rho_b < \rho_a < \rho_f$ (protein $A$ as a repressor) or $\rho_f < \rho_a < \rho_b$ (protein $A$ as an activator).

### A. MDNFL and bistability

In this subsection, we focus on the case $\rho_b < \rho_a < \rho_f$, i.e., the MDNFL motif, and show that such a motif can behave as bistable switches for a wide range of kinetic parameters. For the convenience of analysis, we define $M_a = [M_a]/\rho_a$, $M_s = [M_s]/\rho_a$, $g_s = [g_s]$, and $A = [A]$. With these substitutions, Eqs. (1)– (4) can be rewritten as

$$\frac{dg_s}{dt} = \theta\left(1 - g_s - \frac{A}{A_0}g_s\right), \tag{5}$$

$$\frac{dM_s}{dt} = \rho_0 g_s + \rho_1(1 - g_s) - d_s M_s - \tilde{\gamma} M_a M_s, \tag{6}$$

$$\frac{dM_a}{dt} = 1 - d_m M_a - \tilde{\gamma} M_a M_s, \tag{7}$$

$$\frac{dA}{dt} = \tilde{\beta}_A M_a - d_A A + \theta\left(1 - g_s - \frac{A}{A_0}g_s\right), \tag{8}$$

where $\rho_0 = \rho_f/\rho_a$, $\rho_1 = \rho_b/\rho_a$, $\tilde{\gamma} = \rho_a\gamma$, and $\tilde{\beta}_A = \rho_a\beta_A$. We can calculate the equilibria by setting the right-hand sides of Eqs. (5)– (8) equal to zero and derive the free gene, miRNA, and protein $A$ at an equilibrium as functions of mRNA:

$$g_s = \frac{d_A A_0}{d_A A_0 + \tilde{\beta}_A M_a}, \quad M_s = \frac{\rho_0 d_A A_0 + \rho_1 \tilde{\beta}_A M_a}{(d_s + \tilde{\gamma} M_a)(d_A A_0 + \tilde{\beta}_A M_a)},$$
$$A = \frac{\tilde{\beta}_A M_a}{d_A}. \tag{9}$$

In addition, the mRNA itself satisfies the equation

$$d_m M_a + \frac{(\rho_1 M_a + \rho_0 C_2)M_a}{(M_a + C_1)(M_a + C_2)} = 1, \tag{10}$$

where $C_1 = d_s/\tilde{\gamma}$ and $C_2 = (d_A A_0)/\tilde{\beta}_A$. Obviously, Eq. (10) is equivalent to the following cubic polynomial whose nonnegative roots give the equilibria of $M_a$:

$$M_a^3 + a_2 M_a^2 + a_1 M_a + a_0 = 0, \tag{11}$$

where $a_2 = [(C_1 + C_2)d_m + \rho_1 - 1]/d_m$, $a_1 = (C_1 C_2 d_m + \rho_0 C_2 - C_1 - C_2)/d_m$, and $a_0 = -C_1 C_2/d_m$. We can get the parameter set which guarantees the existence of three positive real roots of Eq. (11) as follows [56,59]:

$$T_a = \{(a_2, a_1, a_0) \in R^3 | a_2 < 0, a_1 > 0, a_0 < 0, A_3 < 0\}, \tag{12}$$

where $A_3 = 27a_0^2 + 4a_0 a_2^3 - 8a_2 a_1 a_0 - a_1^2 a_2^2 + 4a_1^3$. Therefore, the necessary (but not sufficient) conditions for the model with three equilibria are

$$1 + C_1/C_2 - C_1 d_m - \rho_0 < 0 \tag{13}$$

and

$$\rho_1 + (C_1 + C_2)d_m - 1 < 0. \tag{14}$$

More explicitly, Eqs. (13) and (14) can be rewritten as

$$\left(1 + \frac{d_s\beta_A}{A_0 d_A \gamma}\right)\rho_a - \rho_f - \frac{d_s d_m}{\gamma} < 0 \tag{15}$$

and

$$\rho_b - \rho_a + \frac{d_s d_m}{\gamma} + \frac{A_0 d_A d_m}{\beta_A} < 0. \tag{16}$$

Equation (16) means that $\rho_a < \rho_b$ due to $d_s d_m/\gamma + A_0 d_A d_m/\beta_A > 0$. With the previous parameter estimations, we can know that $A_0 d_A d_s d_m/(A_0 d_A \gamma + d_s\beta_A)$ is on the order of $10^{-3}$. Accordingly, we get

$$\rho_a < \frac{\rho_f}{1 + \frac{d_s\beta_A}{A_0 d_A \gamma}} + \frac{A_0 d_A d_s d_m}{A_0 d_A \gamma + d_s\beta_A} \approx \frac{\rho_f}{1 + \frac{d_s\beta_A}{A_0 d_A \gamma}} < \rho_f. \tag{17}$$

Thus, Eqs. (16) and (17) imply $\rho_b < \rho_a < \rho_f$. In other words, the model has three equilibria only when the protein $A$ is a transcriptional repressor.

The bifurcation diagram of the system (1)–(4) as a function of the free $g_s$ promoter transcription rate $\rho_f$ is shown Fig. 4(a). The two saddle-node bifurcation points $SN_1$ ($\rho_f \approx 10.897$) and $SN_2$ ($\rho_f \approx 54.927$) enclose a bistable region. It can be seen that bistability exhibits only for intermediate $\rho_f$ values. The two stable-state branches monotonically decrease with $\rho_f$ because the miRNA concentration increases with $\rho_f$, and thus the unpaired mRNA concentration decreases. For any $\rho_f$ in the bistable region, the system has two stable equilibria, corresponding to low and high values of $A$, respectively, and one unable equilibrium. The stable and unstable branches are represented by solid (red) and dash-dotted (blue) lines, respectively. The system therefore exhibits hysteresis, which is a characteristic of bistable systems. At a specific value of $\rho_f$ in the bistable region, the choice between the stable equilibria is history dependent; i.e., the final state depends on initial conditions [47]. If the value of $\rho_f$ is initially small, the system ends up in the high $A$ state. When moving rightward along the upper stable branch by increasing $\rho_f$, $A$ remains to be in the high state until the bifurcation point $SN_2$ is reached. At this point, a discontinuous jump to a low $A$ state occurs and

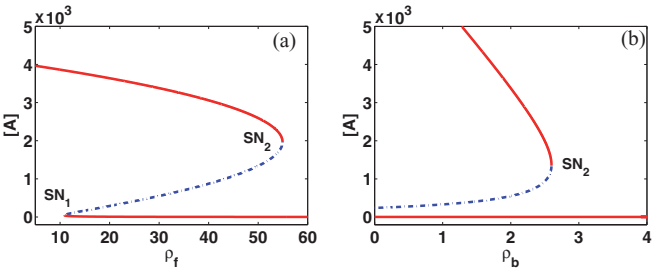


FIG. 4. (Color online) Bifurcation diagrams of the MDNFL model. (a) The bifurcation diagram as a function of $\rho_f$ at $\rho_b = 2$ mol min$^{-1}$. (b) The bifurcation diagram as a function of $\rho_b$ at $\rho_f = 30$ mol min$^{-1}$. Solid and dash-dotted lines denote stable and unstable equilibria, respectively. $SN_1$ and $SN_2$ represent the saddle-node bifurcation points. Other parameter values are $\theta = 0.04$ min$^{-1}$, $[A]_0 = 40$ mol, $\rho_a = 4$ mol min$^{-1}$, $\rho_b = 2$ mol min$^{-1}$, $\beta_A = 1$ min$^{-1}$, $d_s = 0.005$ min$^{-1}$, $d_m = 0.05$ min$^{-1}$, $d_A = 0.01$ min$^{-1}$, and $\gamma = 0.02$ mol$^{-1}$ min$^{-1}$. These parameter values are used as standard values unless otherwise indicated.

the system becomes monostable. If $\rho_f$ is then decreased, the system proceeds along the lower stable branch until $SN_1$ is reached and another discontinuous jump occurs, which brings the system back to the upper stable branch, i.e., a high $A$ state.

In human hematopoietic cells, miR-233 and NFI-A function in a double negative feedback loop to control granulocytic differentiation [22]. In undifferentiated cells, miR-233 level is low and NFI-A level is high; however, upon retinoic acid signaling, miR-233 level increases due to the activation by the TF C/EBPa and NFI-A is then repressed, facilitating the differentiation to the myeloid lineage [22]. These processes can be mathematically represented as an increase in the free $g_s$ promoter transcription rate $\rho_f$. Figure 4(a) shows that when increasing $\rho_f$ from a small value, NFI-A, similar to the $A$ protein, level stays in the upper state until $SN_2$ is reached, where NFI-A switches to a lower state. After that, the NFI-A level will remain in a lower state unless $\rho_f$ is reduced and exceeds the bifurcation point $SN_1$. This double negative feedback loop ensures mutually exclusive expression of miR-233 and NFI-A, thereby generating a bistable system, i.e., undifferentiated versus differentiated hematopoietic cells [22]. Similarly, during skeletal muscle development, Ezh2 and miR-214 form a double negative feedback loop to regulate skeletal muscle cell differentiation [27]. In undifferentiated myoblasts, Ezh2 is highly expressed and represses miR-214. Upon differentiation, MyoD/myogenin expression is activated and promotes transcription of miR-214, which in turn negatively regulates Ezh2 by inhibiting translation of its mRNA and thus reducing Ezh2 expression [27]. These processes can be similarly modeled and discussed.

The bifurcation diagram of system (1)–(4) as a function of parameter $\rho_b$ is shown Fig. 4(b). It indicates that as $\rho_b$ is increased along the upper stable branch, $A$ remains in the high level until $\rho_b$ exceeds some critical value, $SN_2 \approx 2.598$, at which $A$ decreases abruptly to a low value. Then, if $\rho_b$ decreases $A$ stays in its low state indefinitely; i.e., the transition is irreversible. Such a kind of switches is termed irreversible or one-way switches [60]. The one-way switch is an extreme manifestation of hysteresis; i.e., its lower stable solution branches into the negative domain but is actually eliminated due to a physically meaningful restriction. One-way switches presumably play major roles in developmental processes characterized by a point-of-no-return [60]. For instance, frog oocyte maturation in response to progesterone is a particularly clear example [61]. Apoptosis is another decision which must be a one-way switch.

The codimensional two bifurcation diagrams of system (1)–(4) with different control parameters are shown in Fig. 5. The regions enclosed by the solid lines (blue) are bistable regions. It can be seen that bistability occurs only in the region $\rho_b < \rho_b^{cr} \approx 3.70 < \rho_a = 4 < \rho_f^{cr} \approx 8.0 < \rho_f$, i.e., the case of protein $A$ as a transcriptional repressor, which is consistent with the above analysis. In addition, it can be seen that the bistability region becomes wider and the upper threshold of $\rho_f$ increases as $\rho_b$ decreases because a larger $\rho_f$ is needed to compensate inefficiency of the miRNA level at a smaller $\rho_b$ so as to produce bistability, as shown in Fig. 5(a). The bifurcation diagram of system (1)–(4) with $\rho_f$ and $\gamma$ as control parameters is shown in Fig. 5(b). When there is no the negative post-transcriptional regulation, i.e., at $\gamma = 0$, the

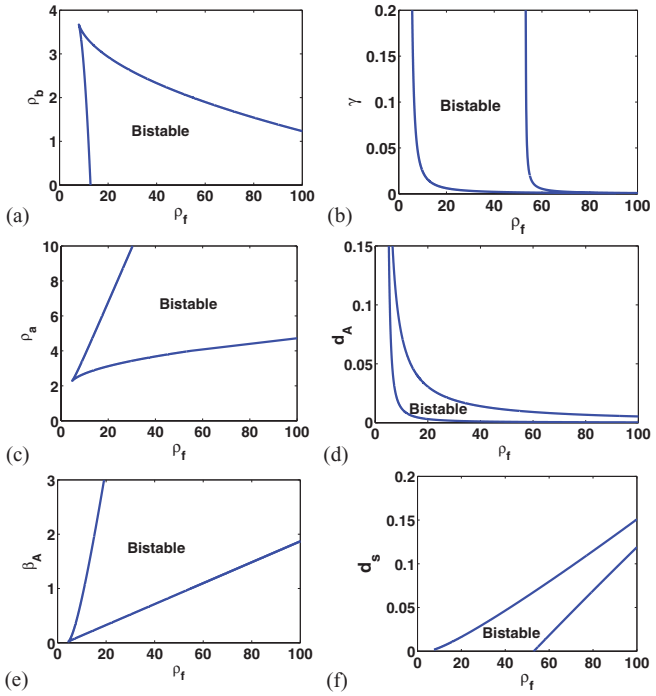


FIG. 5. (Color online) Bifurcation diagrams of the MDNFL model with different control parameters. (a) $\rho_f$ and $\rho_b$ as control parameters. (b) $\rho_f$ and $\gamma$ as control parameters. (c) $\rho_f$ and $\rho_a$ as control parameters. (d) $\rho_f$ and $d_A$ as control parameters. (e) $\rho_f$ and $\beta_A$ as control parameters. (f) $\rho_f$ and $d_s$ as control parameters. The regions enclosed by the solid lines (blue) are bistable regions.

system is monostable. However, moderately increasing $\gamma$ from zero can shift the system into bistability regime. In addition, the bistability region becomes wider with increasing the base pairing rate $\gamma$. A larger miRNA-mRNA base pairing strength $\gamma$ drives the system to the lower $A$ state and so enlarges the bistable region.

In embryologic development, a double negative feedback loop between ZEB1-SIP1 and the miRNA-200 family controls epithelial-mesenchymal transition [18,25]. In epithelial cells, a stable state is maintained by a high miR-200 level, which inhibits ZEB1/SIP1 and hence increases the expression of ZEB-repressed epithelial genes. The transition to a mesenchymal state can be induced by TGF-h, which increases the ZEB1-SIP1 level. A high ZEB1-SIP1 level in turn instigates and maintains a mesenchymal state through the repression of miR-200 by ZEB1-SIP1 [18,25]. These processes can be mathematically represented as an increase in the basal transcription rate $\rho_a$. The bifurcation diagram of system (1)–(4) with $\rho_f$ and $\rho_a$ as control parameters is shown in Fig. 5(c). In agreement with experimental observations, increasing $\rho_a$ from a small value will shift the system from a monomodal low ZEB1/SIP1 state, across a bistable regime, to a monomodal high ZEB1/SIP1 state [25]. In addition, in *Drosophila* eye development, the reciprocal repression between miR-7 and Yan ensures their mutually exclusive expression pattern: Yan is expressed in progenitor cells, and miR-7 is expressed in photoreceptor cells [23]. The transition can be induced by the EGFR signaling, which transiently triggers Yan degradation. A decrease in Yan level relieves miR-7 from transcriptional

repression, subsequently leading to the depletion of Yan in photoreceptor cells [23]. The bifurcation diagram of system (1)–(4) with $\rho_f$ and $d_A$ as control parameters is shown in Fig. 5(d). Increasing the degradation rate $d_A$ from a small value will shift the system from a monomodal high Yan state, across a bistable regime, to a monomodal low Yan state, which induces the transition from a progenitor state to a photoreceptor state [23]. Likewise, during embryonic central nervous system development, a double negative feedback loop between the antineural REST/SCP1 and proneural miR-124 pathways contributes to a rapid and efficient transition of cellular phenotypes between neural progenitors and postmitotic neurons [24]. In nonneuronal cells including neural progenitors, the REST/SCP1 complex transcriptionally represses expression of miR-124 and other neuronal genes. As the REST level decreases during neurogenesis, miR-124 expression is derepressed, and subsequently, miR-124 post-transcriptionally suppresses multiple antineural factors including SCP1, resulting in further inhibition of the antineural pathway by REST/SCP1. The bifurcation diagram the system (1)–(4) with $\rho_f$ and $\beta_A$ as control parameters is shown in Fig. 5(e). Decreasing the production rate $\beta_A$ from a large value will shift the system from a monomodal high REST/SCP1 state, across a bistable regime, to a monomodal low REST/SCP1 state. This regulatory loop may represent key mechanisms to sense the intricate balance between proneural and antineural cues during development, to coordinate robust neuronal gene expression, and to confer neuronal identity in a timely manner [24].

Finally, we study the effect of variations in the degradation rate of miRNA $d_s$ on the dynamics of the system. The bifurcation diagram with $\rho_f$ and $d_s$ as control parameters is shown in Fig. 5(f). With increasing $\rho_f$, bistability emerges, depending on the values of $d_s$. In addition, with increasing $d_s$, the bistability region becomes narrow while the lower and upper thresholds increase moderately. For a fixed $d_s$, when we increase $\rho_f$, the system undergoes a transition from a monomodal high $A$ state to a bistable regime and then to a monomodal low $A$ state.

### B. MSNFL and oscillations

Besides the bistability, miRNA can also induce some nonsteady-state behavior, e.g., the sensitivity and large-amplitude oscillations induced by the miR-17-92 cluster [56]. It was also shown that the effects of miRNAs on gene expression can be destabilizing, i.e., promoting the occurrence of oscillatory expression [62]. In this subsection, we focus on the case $\rho_f < \rho_a < \rho_b$, i.e., the MSNFL motif, and find that such a MSNFL motif can indeed induce destabilizing effects by producing oscillations for wide ranges of kinetic parameters.

When $A$ is a transcriptional activator, the base pairing of miRNA $M_s$ with mRNA $M_a$ forms a negative feedback and can serve to diminish the variation in the miRNA concentration when $A$ varies. The negative feedback may lead to oscillations when the transcription rate of $M_a$ lies in the intermediate range $\rho_f < \rho_a < \rho_b$. Intuitively, when the concentrations of $A$ and $M_s$ are low, no $A$ is bound to the $g_s$ promoter, and the transcription rate of miRNA is lower than that of mRNA and the codegradation cannot prevent the increase of $M_a$ concentration and further $A$ concentration. When the concentration of $A$ has reached a critical level, $A$ begins to bind to the $g_s$ promoter and activate the transcription of miRNA, which results in a higher transcription rate of $M_s$ than that of $M_a$ and the diminution of free $M_a$ by codegradation. Since the mRNA concentration is high, the transcribed miRNA base pairs rapidly with mRNA and degrades, the concentration of unpaired miRNA becomes low. Eventually, the concentration of $A$ drops, due to the diminution of free $M_a$, below the binding level and no longer activates the $g_s$ transcription. $M_s$ continues to be transcribed from the $g_s$ for a while, and since few mRNA are present, low concentration of mRNA leads to a rise of the concentration of free miRNA. Finally, the concentration of $M_s$ drops and a new cycle starts with low concentrations of $A$ and $M_s$, as shown in Fig. 6(a).

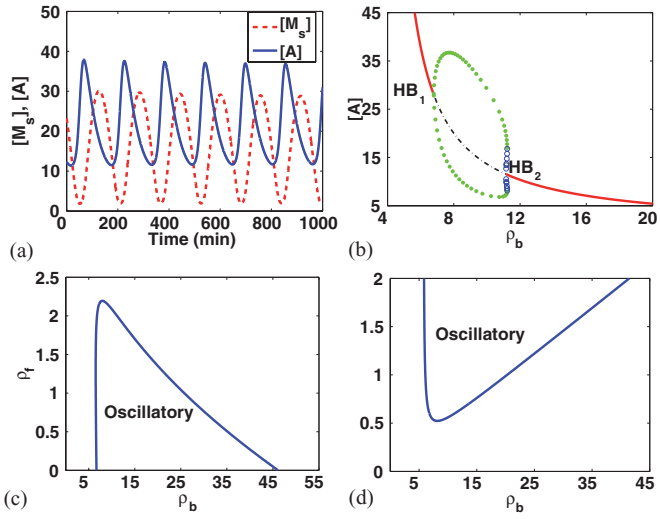


FIG. 6. (Color online) The dynamics of the MSNFL model. (a) Sustained oscillations of the miRNA and protein. (b) The bifurcation diagram with $\rho_b$ as a control parameter, where $HB_1$ and $HB_2$ denote Hopf bifurcation points, and solid (open) circles surrounding the unstable state represent the maxima and minima of $[A]$ during a stable (an unstable) oscillation. (c) The bifurcation diagram with $\rho_b$ and $\rho_f$ as control parameters. (d) The bifurcation diagram with $\rho_b$ and $\gamma$ as control parameters. The regions enclosed by solid lines (blue) are the oscillatory regions. The parameter values are $\rho_f = 2$ mol min$^{-1}$, $\rho_b = 8$ mol min$^{-1}$, $\beta_A = 0.5$ min$^{-1}$, $d_A = 0.02$ min$^{-1}$, and $\gamma = 0.6$ mol$^{-1}$ min$^{-1}$. Other parameters are the same as those used in Fig. 4.

The bifurcation diagrams of the system (1)–(4) are shown in Fig. 6. It can be seen that oscillations are favored for intermediate values of $\rho_b$, as shown in Fig. 6(b). The system displays successively a stable equilibrium with a high $A$ level, a stable oscillatory state, and finally a stable equilibrium with a low $A$ level as $\rho_b$ increases. There exist a supercritical Hopf bifurcation $HB_1$ at $\rho_b \approx 6.792$ and a subcritical Hopf bifurcation $HB_2$ at $\rho_b \approx 11.15$. In addition, stable oscillation and equilibrium may coexist for values of $\rho_b$ in the interval enclosed by $HB_2$ and a fold limit cycle bifurcation ($\rho_b \approx 11.22$) due to the occurrence of the subcritical Hopf bifurcation. The conditions under which the system (1)–(4) exhibits Hopf bifurcations can be similarly derived by using the method employed in Ref. [63], and we will not repeat here.

The bifurcation diagram of system (1)–(4) with $\rho_f$ and $\rho_b$ as control parameters is shown in Fig. 6(c). The region

enclosed by the solid line (blue) is the oscillatory region. Consistent with the above analysis, it can be seen that to make the system oscillatory, the free $g_s$ promoter transcription rate $\rho_f$ must be smaller than the $M_a$ transcription rate $\rho_a$. For a fixed value of $\rho_b$, there exists a maximum value of $\rho_f$, $\rho_f^{\max}$, beyond which oscillations do not occur. With decreasing $\rho_b$, the oscillatory region becomes larger and the upper threshold of $\rho_f$ increases moderately because a larger $\rho_f$ is needed to compensate the inefficiency in the miRNA level, due to a smaller $\rho_b$, to produce oscillations. The bifurcation diagram of system (1)–(4) with $\gamma$ and $\rho_b$ as control parameters is shown in Fig. 6(d). When the base pairing rate $\gamma$ is too small, the system will converge to a stable equilibrium and no oscillations occur, which means codegradation rate must be sufficiently large to induce oscillations. As the base pairing rate $\gamma$ increases, the oscillatory region becomes wider. Therefore, the miRNA-mediated negative regulation can indeed induce destabilizing effects by producing oscillations.

## IV. DISCUSSION AND CONCLUSION

The miRNA-mediated post-transcriptional regulation plays critical roles in almost every cellular process, and changes in proteins may result in developmental disorders and diseases such as cancer. Of particular relevance is the accumulating evidence that the interplay of miRNAs and transcriptional regulators such as activators and repressors regulates key developmental events and cell fate decisions [11–19]. Computational and experimental studies have identified an abundance of motifs involving miRNAs and TFs [11–31]. The simplest one is a two-node MFL in which a TF regulates an miRNA and the TF itself is negatively regulated by the miRNA. The MFL can be classified into two classes: MDNFLs and MSNFLs, depending on the kinds of transcriptional regulations. These two kinds have been reported in several recent studies [21–31]. In this paper, we present a general computational model for the MFL based on biochemical regulations and explore its dynamics by using bifurcation analysis. The MFL can behave as bistable switches or oscillators, depending on the TF as a repressor or an activator. In agreement with experimental observations, the model can account for many functional features of miRNAs in fate decisions such as proliferation, differentiation, and apoptosis during development.

Bistability, i.e., the capacity to choose between two different stable states, is an essential feature of cellular systems from bacteriophage λ to mammals and has been extensively studied from both theoretical and experimental viewpoints [47]. Positive feedback and cooperativity in the regulation of gene expression are generally considered to be necessary for obtaining bistable expression states [48,64]. It is interesting to note that, in our model, we assume that the production of miRNA, $M_s$, is regulated by protein $A$, through binding of a single protein $A$ to its promoter, $g_s$, that is, without cooperative binding of the TF to its promoter. In this case, the system is always monostable if the miRNA-mediated regulation does not exist [48,64]. On the other hand, the miRNA-mediated regulation, if it works solely, also leads to monostability [57]. Surprisingly, under the interplay of the TF and miRNA, it can be found that the MDNFL model can behave as switches for wide ranges of parameters even without cooperative binding. It thus provides a novel mechanism to induce bistability through this combinatorial regulation even without cooperativity in the regulation, which is fundamentally distinct from the generation of bistability by intrinsically nonlinear positive feedback regulation, such as protein dimerization and cooperative formation of heterodimers [47,48,51,65]. The evidence for use of the MDNFL motif as switches has been reported recently, especially on cell fate decisions [22–29]. We hope this novel mechanism can be realized in artificial genetic networks in the future.

On the other hand, oscillations also occur in many contexts such as metabolism, signaling, and development and control many important aspects of cell physiology such as circadian rhythms, DNA synthesis, mitosis, and development of somites in vertebrate embryos [49]. The minimum requirement for oscillations is a negative feedback loop with a time delay [66]. There are several ways to produce an effective time delay. Here we incorporate mRNA dynamics to explicitly describe the processes of transcription and translation, and show that the MSNFL model can produce oscillations for wide ranges of parameters. It should be stressed that the oscillations induced by the miRNA in the MSNFL model require neither an additional positive feedback loop, nor self-activation of the gene, nor cooperative binding of the TF, nor saturated degradation [49,67]. Therefore, it may provide a general network structure to produce oscillations. However, the evidence for the use of MSNFL motif as oscillators appears less clear-cut at present, which may be due to the fact that the possible roles of the MSNFL modules as oscillators were not fully realized before. It is therefore expected that this study will hopefully help trigger further experimental investigations.

We have presented that the miRNA-mediated motif is able to behave as switches or oscillators. It has been shown that excitability may occur in systems with combined positive and negative feedback loops [68,69], exemplified by a transient differentiation into competence in *Bacillus subtilis* [70–72]. However, we did not find excitability under the given parameter values. Whether excitable dynamics can occur in the miRNA-mediated motif still remains to be determined.

Besides the simplest architecture discussed here, miRNA-mediated network motifs with other architectures can be similarly analyzed, such as miRNA-mediated single-input modules in which an miRNA regulates a group of target genes [13] and miRNA-mediated feedback and feed-forward loops [11,12,15,16,73]. The insight gained from the study of these simple motifs is expected to provide a basis for the investigation of more complex networks assembled by simple building blocks. A more clear understanding of the miRNA-mediated motifs is also important for bio-engineering or artificial control of specified components, interactions, and even network functions. It is hoped that the results presented here can provide a new view on how gene expression is regulated and further guidance for experiments. In addition, it has been suggested that it would be cost effective for cells to use miRNA-mediated post-transcriptional regulations because these small molecules do not need to be translated, which makes energetic cost of their synthesis smaller in comparison with synthesis of regulatory proteins [74]. Given these advantages of miRNAs, it is not surprising why miRNAs are so widespread in almost every cellular process. Moreover, it has recently been shown that manipulation of miRNAs

is readily achievable *in vivo* and holds exciting promise for potential therapeutic applications for diseases associated miRNAs [75,76].

Finally, it should be pointed out that cellular processes at the molecular level are inherently stochastic [77]. The origin of stochasticity can be attributed to random transitions among discrete biochemical states, which are the source of inherent fluctuations. It has been shown that noise may induce bistability or oscillations which are not present in the deterministic model [64,78], or induce bifurcations which have no counterpart in the deterministic descriptions [79]. Future studies should thus focus on how stochastic noise affects dynamics of the miRNA-mediated regulation.

## ACKNOWLEDGMENTS

This work was supported by the National Science Foundation of China (Grants No. 11171206, 11172158, and 10832006), Innovation Program of Shanghai Municipal Education Commission (No.12YZ030), and Shanghai University Graduate Innovation Funds (Grant No. SHUCX111025).

## APPENDIX

When participating in cellular processes, miRNAs mainly mediate mRNA degradation or translational repression [7–10]. As discussed in the main text, we develop our model by just considering miRNA-mediated mRNA degradation. In this Appendix, we will show that the results for the miRNA-mediated mRNA degradation are qualitatively similar to the miRNA-mediated translational repression by a specified example. Similar to the miRNA-mediated mRNA degradation, we use just a relatively simple manner to model the translation repression as follows:

$$\frac{d[g_s]}{dt} = \theta[g_s : A] - \alpha[g_s][A], \tag{A1}$$

$$\frac{d[M_s]}{dt} = \rho_f[g_s] + \rho_b[g_s : A] - d_s[M_s] - \gamma[A][M_s], \tag{A2}$$

$$\frac{d[M_a]}{dt} = \rho_a - d_m[M_a], \tag{A3}$$

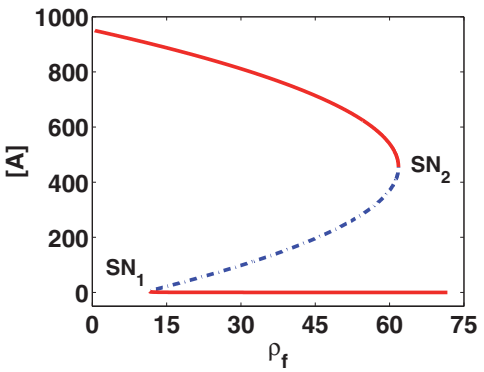


FIG. 7. (Color online) The bifurcation diagram of the system (A1)–(A4) as a function of $\rho_f$. The parameters are $\rho_a = 1$ mol min$^{-1}$, $\rho_b = 0.5$ min$^{-1}$, and $\beta_A = 0.5$ min$^{-1}$. Other parameters are the same as those used in Fig. 4. Solid and dash-dotted lines denote stable and unstable equilibria, respectively. Two saddle-node bifurcation points are denoted by $SN_1$ and $SN_2$.

$$\frac{d[A]}{dt} = \beta_A[M_a] - d_A[A] - \gamma[A][M_s] + \theta[g_s : A] - \alpha[A][g_s], \tag{A4}$$

where $\gamma$ denotes the association rate of the miRNA and protein. In other words, the miRNA and protein codegrade nonlinearly at a rate $\gamma$ besides their respective linear degradation.

The bifurcation diagram of system (A1)–(A4) as a function of the free $g_s$ promoter transcription rate $\rho_f$ is shown in Fig. 7. Two saddle-node bifurcation points $SN_1$ ($\rho_f \approx 11.565$) and $SN_2$ ($\rho_f \approx 61.793$) enclose a bistable region, indicating that the translational repression can also induce bistability. In other words, both of the miRNA-mediated scenarios can induce bistability. The only difference between the two scenarios is that the upper threshold of $\rho_f$ for the translational repression may be smaller than that for the miRNA-mediated mRNA degradation due to a much faster degradation in the protein levels induced by the translational repression, as shown in Ref. [51].

[1] S. Gottesman, Annu. Rev. Microbiol. **58**, 303 (2004).
[2] L. S. Waters and G. Storz, Cell **136**, 615 (2009).
[3] A. S. Flynt and E. C. Lai, Nat. Rev. Genet. **9**, 831 (2008).
[4] V. Ambros, Nature (London) **431**, 350 (2004).
[5] G. Stefani and F. J. Slack, Nat. Rev. Mol. Cell. Biol. **9**, 219 (2008).
[6] N. Bushati and S. M. Cohen, Annu. Rev. Cell Dev. Biol. **23**, 175 (2007).
[7] W. Filipowicz, S. N. Bhattacharyya, and N. Sonenberg, Nat. Rev. Genet. **9**, 102 (2008).
[8] D. P. Bartel, Cell **116**, 281 (2004).
[9] M. A. Valencia-Sanchez, J. Liu, G. J. Hannon, and R. Parker, Genes Dev. **20**, 515 (2006).
[10] H. Guo, N. T. Ingolia, J. S. Weissman, and D. P. Bartel, Nature (London) **466**, 835 (2010).
[11] J. Tsang, J. Zhu, and A. van Oudenaarden, Mol. Cell. **26**, 753 (2007).
[12] R. Shalgi, D. Lieber, M. Oren, and Y. Pilpel, PLoS Comput. Biol. **3**, e131 (2007).
[13] Y. Shimoni, G. Friedlander, G. Hetzroni, G. Niv, S. Altuvia, O. Biham, and H. Margalit, Mol. Syst. Biol. **3**, 138 (2007).
[14] X. Yu, J. Lin, D. J. Zack, J. T. Mendell, and J. Qian, Nucleic Acids Res. **36**, 6494 (2008).
[15] A. Re, D. Corá, D. Taverna, and M. Caselle, Mol. BioSyst. **5**, 854 (2009).
[16] N. J. Martinez *et al.*, Genes Dev. **22**, 2535 (2008).

[17] N. J. Martinez and A. J. M. Walhout, BioEssays **31**, 435 (2009).
[18] M. Inui, G. Martello, and S. Piccolo, Nat. Rev. Mol. Cell. Biol. **11**, 252 (2010).
[19] K. N. Ivey and D. Srivastava, Cell Stem Cell **7**, 36 (2010).
[20] R. J. Johnston, S. Chang, J. F. Etchberger, C. O. Ortiz, and O. Hobert, Proc. Natl. Acad. Sci. USA **102**, 12449 (2005).
[21] J. Kim *et al*., Science **317**, 1220 (2007).
[22] F. Fazi *et al*., Cell **123**, 819 (2005).
[23] X. Li and R. W. Carthew, Cell **123**, 1267 (2005).
[24] J. Visvanathan, S. Lee, B. Lee, J. W. Lee, and S.-K. Lee, Genes Dev. **21**, 744 (2007).
[25] C. P. Bracken *et al*., Cancer Res. **68**, 7846 (2008).
[26] N. Xu, T. Papagiannakopoulos, G. Pan, J. A. Thomson, and K. S. Kosik, Cell **137**, 647 (2009).
[27] A. H. Juan, R. M. Kumar, J. G. Marx, R. A. Young, and V. Sartorelli, Mol. Cell. **36**, 61 (2009).
[28] C. Zhao, G. Sun, S. Li, and Y. Shi, Nat. Struct., Mol. Biol. **16**, 365 (2009).
[29] V. Pospisil *et al*., EMBO J. **30**, 4450 (2011).
[30] H. Zhao, A. Kalota, S. Jin, and A. M. Gewirtz, Blood **113**, 505 (2009).
[31] Z. Yu *et al*., J. Cell Biol. **182**, 509 (2008).
[32] S. L. Bumgarner, R. D. Dowell, P. Grisafi, D. K. Gifford, and G. R. Fink, Proc. Natl. Acad. Sci. USA **106**, 18321 (2009).
[33] D. Iliopoulos, H. A. Hirsch, and K. Struhl, Cell **139**, 693 (2009).
[34] S. S. Shen-Orr, R. Milon, S. Mangan, and U. Alon, Nat. Genet. **31**, 64 (2002).
[35] T. I. Lee *et al*., Science **298**, 799 (2002).
[36] U. Alon, Nat. Rev. Genet. **8**, 450 (2007).
[37] D. Nevozhay, R. M. Adams, K. F. Murphy, K. Josić, and G. Balázsi, Proc. Natl. Acad. Sci. USA **106**, 5123 (2009).
[38] L. Goentoro, O. Shoval, M. W. Kirschner, and U. Alon, Mol. Cell **36**, 894 (2009).
[39] N. Rosenfeld, M. B. Elowitz, and U. Alon, J. Mol. Biol. **323**, 785 (2002).
[40] S. Mangan, A. Zaslaver, and U. Alon, J. Mol. Biol. **334**, 197 (2003).
[41] S. Mangan and U. Alon, Proc. Natl. Acad. Sci. USA **100**, 11980 (2003).
[42] S. Mangan, S. Itzkovitz, A. Zaslaver, and U. Alon, J. Mol. Biol. **356**, 1073 (2006).
[43] R. J. Prill, P. A. Iglesias, and A. Levchenko, PLoS Biol. **3**, e343 (2005).
[44] R. Milo *et al*., Science **298**, 824 (2002).
[45] T. S. Gardner, C. R. Cantor, and J. J. Collins, Nature (London) **403**, 339 (2000).
[46] E. M. Ozbudak, M. Thattai, H. N. Lim, B. I. Shraiman, and A. van Oudenaarden, Nature (London) **427**, 737 (2004).
[47] J. E. Ferrell, Curr. Opin. Cell. Biol. **14**, 140 (2002).
[48] J. E. Ferrell and W. Xiong, Chaos **11**, 227 (2001).
[49] B. Novák and J. J. Tyson, Nat. Rev. Mol. Cell Biol. **9**, 981 (2008).
[50] P. Francois and V. Hakim, Phys. Rev. E **72**, 031908 (2005).
[51] D. Liu, X. Chang, Z. Liu, L. Chen, and R. Wang, PLoS ONE **6**, e17029 (2011).
[52] Y. Wang, C. L. Liu, J. D. Storey, R. J. Tibshirani, D. Herschlag, and P. O. Brown, Proc. Natl. Acad. Sci. USA **99**, 5860 (2002).
[53] M. Kaern, T. C. Elston, W. J. Blake, and J. J. Collins, Nat. Rev. Genet. **6**, 451 (2005).
[54] M. H. Glickman and A. Ciechanover, Physiol. Rev. **82**, 373 (2002).
[55] R. Khanin and V. Vinciotti, J. Comput. Biol. **15**, 305 (2008).
[56] B. D. Aguda, Y. Kim, M. G. Piper-Hunter, A. Friedman, and C. B. Marsh, Proc. Natl. Acad. Sci. USA **105**, 19678 (2008).
[57] E. Levine, Z. Zhang, T. Kuhlman, and T. Hwa, PLoS Biol. **5**, e229 (2007).
[58] E. Levine and T. Hwa, Curr. Opin. Microbiol. **11**, 574 (2008).
[59] B. D. Aguda and B. L. Clarke, J. Chem. Phys. **87**, 3461 (1987).
[60] J. J. Tyson, K. C. Chen, and B. Novak, Curr. Opin. Cell. Biol. **15**, 221 (2003).
[61] J. E. Ferrell and E. M. Machleder, Science **280**, 895 (1998).
[62] Z. R. Xie, H. T. Yang, W. C. Liu, and M. J. Hwang, Biochem. Biophys. Res. Commun. **358**, 722 (2007).
[63] R. Wang, Z. Jing, and L. Chen, Bull. Math. Biol. **67**, 339 (2005).
[64] A. Lipshtat, A. Loinger, N. Q. Balaban, and O. Biham, Phys. Rev. Lett. **96**, 188101 (2006).
[65] V. P. Zhadanov, BioSystems **95**, 75 (2009).
[66] B. Mengel, A. Hunziker, L. Pedersen, A. Trusina, M. H. Jensen, and S. Krishna, Curr. Opin. Genet. Dev. **20**, 656 (2010).
[67] K. Sneppen, S. Krishna, and S. Semsey, Annu. Rev. Biophys. **39**, 43 (2010).
[68] X. J. Tian, X. P. Zhang, F. Liu, and W. Wang, Phys. Rev. E **80**, 011926 (2009).
[69] B. Pfeuty and K. Kaneko, Phys. Biol. **6**, 046013 (2009).
[70] G. M. Süel, J. Garcia-Ojalvo, L. M. Liberman, and M. B. Elowitz, Nature (London) **440**, 545 (2006).
[71] G. M. Süel, R. P. Kulkaryni, J. Dworkin, J. Garcia-Ojalvo, and M. B. Elowitz, Science **315**, 1716 (2007).
[72] H. Maamar, A. Raj, and D. Dubnau, Science **317**, 526 (2007).
[73] N. Mitarai, A. M. C. Andersson, S. Krishna, S. Semsey, and K. Sneppen, Phys. Biol. **4**, 164 (2007).
[74] S. Altuvia and E. G. Wagner, Proc. Natl. Acad. Sci. USA **97**, 9824 (2000).
[75] J. Krützfeldt *et al*., Nature (London) **438**, 685 (2005).
[76] J. Elmén *et al*., Nature (London) **452**, 896 (2008).
[77] G. Balázsi, A. van Oudenaarden, and J. J. Collins, Cell **144**, 910 (2011).
[78] J. M. Vilar, H. Y. Kueh, N. Barkai, and S. Leibler, Proc. Natl. Acad. Sci. USA **99**, 5988 (2002).
[79] T. B. Kepler and T. C. Elston, Biophys. J. **81**, 3116 (2001).